Pergamon

Int. J. Heat Mass Transfer. Vol. 38, No. 1, pp. 113–126, 1995

0017-9310/95 $9.50+0.00

0017-9310(94)00124-3

Thermal convection in small enclosures: an atypical bifurcation sequence

D. MUKUTMONI
Adapco, 60 Broadhollow Road, Melville, NY 11747, U.S.A.

and

K. T. YANG
Department of Aerospace and Mechanical Engineering, University of Notre Dame, Notre Dame, IN 46556, U.S.A.

(*Received* 2 *August* 1993 *and in final form* 4 *April* 1994)

Abstract—The present numerical study examines bifurcation sequences in Rayleigh–Bénard convection for small aspect ratio enclosures. The three-dimensional rectangular enclosure has insulated sidewalls. The top wall is cooled and the bottom wall is heated, both isothermally. The Boussinesq approximation is invoked with the exception of temperature dependent viscosity of the fluid. The numerical simulations closely model specific experiments. Accordingly, the mean Prandtl number is set to 5 and the aspect ratios are set to 2.42 and 1.23. The computations exactly match the bifurcation sequence observed in the experiments while increasing the Rayleigh number, which is steady state → periodic → quasi-periodic → steady state. It is established that the counter-intuitive transition from quasi-periodic to steady dynamical behavior with an increase in Rayleigh number is due to spatial changes in the mean velocity and temperature fields that accompany the bifurcation. The computations span a range of Rayleigh numbers from 2.5×10^3 to 1.3×10^5. Both unsteady and steady thermal convection are examined in detail.

INTRODUCTION

Rayleigh–Bénard convection is a heavily investigated area due to its extensive theoretical relevance and practical applications. This work represents a continuation of our past efforts to investigate the dynamical behavior of Rayleigh–Bénard convection in small aspect ratio enclosures [1–3]. In past works and in the present, the Prandtl number of the fluid and aspect ratios were fixed and the effect of the Rayleigh number was studied.

The Rayleigh–Bénard (referred to as RB for convenience) convection in small aspect ratio rectangular parallelepiped enclosures referred to here comprises the following physical constraints:

(1) isothermal top and bottom walls with the bottom wall heated and the top wall cooled;
(2) adiabatic vertical side walls.

As noted by several experimentalists [4, 5] and numerical studies [1–3, 6], the RB system starts with a motionless conduction domain below a certain critical Rayleigh number that is a function of the aspect ratios. As the Rayleigh number is increased, steady and time-independent convection ensues. Further increases in the Rayleigh number result in discrete flow transitions that increases the spatio-temporal complexity of the flow and temperature field, finally leading to turbulent flow. For instance, in the case documented numerically by Mukutmoni and Yang [2, 3], the flow field undergoes the following sequence of changes: steady state → periodic → quasi-periodic → chaotic.

In an extensive set of experiments, Gollub and Benson [4] showed that there are several routes to turbulent convection for the RB system in small boxes (aspect ratios less than 5). The general trend reported was that increasing the Rayleigh number led to an increasingly dynamically complex behavior (via discrete transitions) as noted in the simulations. However, one anomalous set of results was recorded.

For aspect ratios of 2.42 and 1.23 and for a mean Prandtl number of 5, Gollub and Benson [4] observed the following dynamical sequence: steady-state → periodic → quasi-periodic → steady state. This reversion to steady state was very unexpected and could not be explained in the experiments which, for the most part, were velocity measurements at a given point using LDV techniques.

In this set of computations, we attempted to simulate the anomalous bifurcation sequence noted in their experiments. If successful, the greater degree of flow details available would let us gain further insight into the physics of the transition. We hoped that the details of the phenomena would let us satisfactorily explain the rather counter-intuitive reversion to steady state from quasi-periodicity when the Rayleigh number is increased. At the same time, the calculations would let us take a closer and a more detailed look at flow

NOMENCLATURE

A_x	aspect ratio in the x-direction, L_x/L
A_z	aspect ratio in the z-direction, L_z/L
g	acceleration due to gravity [m s^{-2}]
L	height of the enclosure [m]
L_x	dimension of the enclosure in the x-direction [m]
L_z	dimension of the enclosure in the z-direction [m]
Nu	Nusselt number
p	nondimensional pressure, scaled by $\rho\alpha^2/L_2$
Pr	Prandtl number, ν/α
Ra	$g\beta\Delta TL^3/\nu\alpha$, Rayleigh number
Ra_c	critical Rayleigh number
t	nondimensional time, scaled by L^2/α
T	nondimensional temperature, scaled by ΔT
T_C	cold wall temperature [°C]
T_H	hot wall temperature [°C]
ΔT	temperature difference, $T_H - T_C$ [°C]
U	nondimensional velocity vector, scaled by α/L
u	nondimensional x-direction velocity, scaled by α/L
v	nondimensional y-direction velocity, scaled by α/L
w	nondimensional z-direction velocity, scaled by α/L
x	nondimensional horizontal spatial co-ordinate, scaled by L
y	nondimensional vertical spatial co-ordinate, scaled by L
z	nondimensional spatial co-ordinate in the direction of depth, scaled by L.

Greek symbols

α	thermal diffusivity [m^2 s^{-1}]
β	coefficient of volume expansion, $1/K$
ε	nondimensional perturbation parameter, $(Ra/Ra_c)-1$
ν	dynamic viscosity [m^2 s^{-1}]
ρ	density [kg m^{-3}].

and temperature fields over a wide range of Rayleigh numbers that span steady and unsteady thermal convection regimes.

This paper begins with a discussion on the formulation of the problem and validation of the code. This is followed by a description of the results in the subcritical steady convection regime. The subsequent sections describe the computations in the periodic and quasi-periodic regimes and the reversion to steady state from quasi-periodicity. The final sets of results are preliminary simulations in the Rayleigh number range beyond the second steady state. This paper ends with a summary of the major conclusions.

FORMULATION AND CODE VALIDATION

The experimental conditions given in Gollub and Benson [4] are matched as closely as possible. The geometry of the enclosure is shown in Fig. 1. The dependent and independent variables are normalized by the standard thermal diffusion scales and the height of the enclosure. The temperature is normalized such that it is set to 0.5 at the bottom wall and -0.5 at the top wall. Further details are given in the Nomenclature. The dimensions of the experimental enclosure [4] are 14.66 by 28.85 by 11.94 mm high, which leads to aspect ratios of 2.42 and 1.23 in each of the horizontal directions. The Boussinesq approximation is used with the exception of the temperature-dependent viscosity. The maximum temperature difference between the top and bottom plate is of the order of several degrees. In that range, the viscosity of water, the working fluid, varies by a maximum of 6%. The rest of the transport properties vary by less than 1%. So, it is reasonable to assume that all transport properties are constant with the exception of the viscosity, which is a function of the temperature. The average Prandtl number is set to 5.00, in order to match experimental conditions [4].

The nondimensionalized governing equations for the Boussinesq equations are the following [7]:

$$\nabla \cdot \mathbf{U} = 0 \tag{1}$$

$$\frac{\partial u}{\partial t} + \nabla \cdot (u\mathbf{U}) = -\frac{\partial p}{\partial x} + \nabla \cdot (Pr\,\nabla u) \tag{2}$$

$$\frac{\partial v}{\partial t} + \nabla \cdot (v\mathbf{U}) = -\frac{\partial p}{\partial y} + \nabla \cdot (Pr\,\nabla v) + Ra\,Pr\,T \tag{3}$$

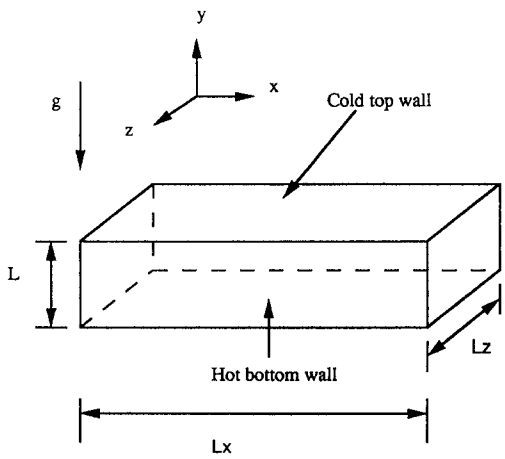

Fig. 1. Geometry of enclosure and co-ordinate system.

$$\frac{\partial w}{\partial t}+\nabla\cdot(w\mathbf{U})=-\frac{\partial p}{\partial z}+\nabla\cdot(Pr\nabla w) \quad (4)$$

$$\frac{\partial T}{\partial t}+\nabla\cdot(T\mathbf{U})=\nabla^2 T. \quad (5)$$

The boundary conditions are the following:

$$x=0, A_x;$$

$$0\leqslant z\leqslant A_z, 0\leqslant y\leqslant 1 \quad u=v=w=0\frac{\partial T}{\partial x}=0 \quad (6)$$

$$z=0, A_z;$$

$$0\leqslant x\leqslant A_x, 0\leqslant y\leqslant 1 \quad u=v=w=0\frac{\partial T}{\partial z}=0 \quad (7)$$

$$y=0,1;$$

$$0\leqslant x\leqslant A_x, 0\leqslant z\leqslant A_z \quad u=v=w=0 \quad T=0.5-y. \quad (8)$$

The temperature-dependent viscosity which is the Prandtl number in the nondimensional formulation is the following, based on a polynomial curve fit of the data tabulated in Incropera and DeWitt [8] for the temperature range between 7 and 87°C for water:

$$Pr(T)=12.316-0.33877T+4.2331\times10^{-3}T^2-1.967\times10^{-5}T^3. \quad (9)$$

The mean volume averaged Prandtl number was taken as 5.00, which corresponds to a mean temperature (average of top and bottom wall temperatures) of around 33°C. The temperature T is dimensional (°C) for equation (9) alone.

The governing nonlinear partial differential equations are solved using the control (finite) volume method, QUICK scheme and SIMPLEX algorithm. Details are given in Mukutmoni and Yang [1]. A first order implicit backward-Euler scheme is used. However, the time stepping is chosen rather conservatively. The minimum explicit time step based on the CFL criteria is calculated for each control volume and this is never exceeded in all the calculations. Typically, the time step chosen was varied between one-fifth and one-third of the explicit limit.

An exhaustive validation and grid refinement study has been reported for RB convection in Mukutmoni and Yang [2]. The study [2] recommends that as a compromise between accuracy and computer resources, an average nondimensional horizontal resolution of 0.1 units be observed, along with a resolution of 0.05 units in the vertical direction. Since the Rayleigh numbers computed are higher for the present study, this average resolution is reduced further. As shown in Fig. 2, a $34\times30\times24$ nonuniform grid is used in the x-, y- and z-directions, respectively, for a 2.4 : 1 : 1.2 box.

COMPARISON WITH LINEAR STABILITY THEORY

The computational results are consistent with some theoretical results near the critical Rayleigh number for the onset of convection. The critical Rayleigh number as a function of the aspect ratios is now well established through linear stability theory and has been compiled and tabulated in Holland and Raithby [9]. This can be checked indirectly by numerical simulation. Other well-established theoretical results are:

(1) The average magnitude of the velocity is proportional to the square root of the parameter ε [10], where $\varepsilon=(Ra/Ra_c)-1$ near the critical point in the supercritical region. This implies that the average kinetic energy would be proportional to ε.

(2) The average Nusselt number is a linear function of the parameter ε [11].

A comparison with results near the onset of convection indicates that there is qualitative and quantitative agreement between the analytical results for these limiting cases. The calculations are carried out for the same geometry and using the same grid. In Fig. 3(a), the volume-averaged kinetic energy as a function of the Rayleigh number has been plotted near the critical Rayleigh number. Similarly, in Fig. 3(b), the average Nusselt number over any horizontal cross section (they should all be the same for steady-state conditions due to conservation of thermal energy) is plotted as a function of the Rayleigh number. In both cases, the limiting behavior is linear and consistent with theoretical results. The critical Rayleigh number is estimated to be close to 2420 by extrapolation to a vanishingly small kinetic energy and a Nusselt number of unity. This is consistent with the stability results given in Holland and Raithby [11] and presented in Table 1 for comparison. As seen in Table 1, the exact aspect ratios of the present case were not tabulated in ref. [11]. However, the critical Rayleigh number is within bounds of the published results for the aspect ratios closest to the one in this article.

STEADY AND OSCILLATORY CONVECTION

According to the experiments of Gollub and Benson [4], the bifurcation phenomena depend not only on the parameters (Rayleigh number, Prandtl number and aspect ratios), but also on the initial conditions. In the subcritical range (before the first bifurcation), it is therefore natural that we match the time-independent flow field of the experiments. If the flow field is regular like a roll, it is possible to generate the required flow structure using sinusoidal velocity perturbations as initial conditions. This was done in Mukutmoni and Yang [1], and the same technique is used here as well.

For the present set of experiments, a two-roll pattern parallel to the short side was the required mean flow. In Fig. 4(a), the flow field at the vertical mid-section perpendicular to the roll axis is shown in terms of the velocity vectors at a Rayleigh number of 4×10^4. The flow consists of two steady, symmetric and coun-

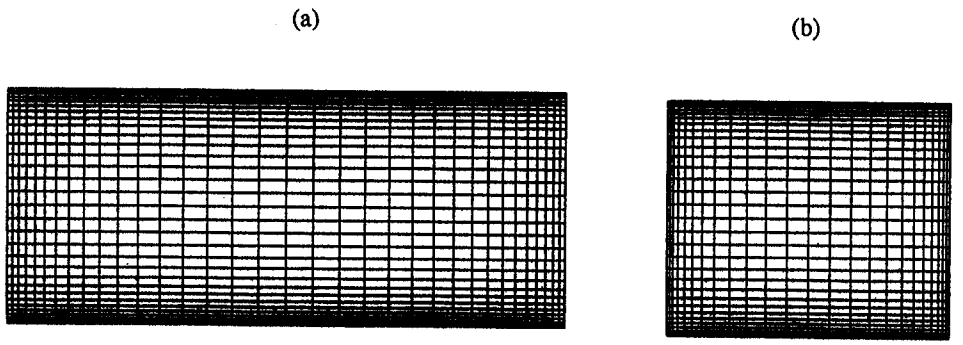

Fig. 2. Nonuniform grid of the computational domain: (a) x–y plane; and (b) z–y plane.

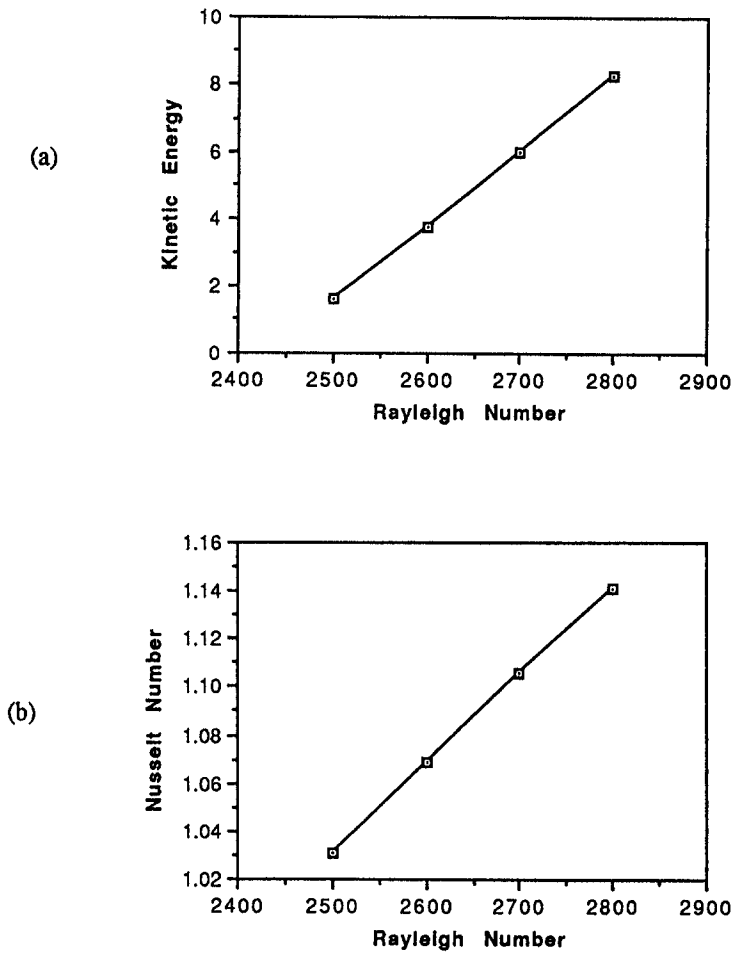

Fig. 3. (a) Volume averaged kinetic energy as a function of Rayleigh number; and (b) average Nusselt number over a horizontal cross-section as a function of Rayleigh number.

ter-rotating rolls that are mostly two-dimensional. Figure 4(b) shows the velocity field at vertical mid-section parallel to the roll axis. The velocity vectors show that the three-dimensional effects are confined to the side-walls only.

The contours of the temperature field show the same quasi two-dimensional structure. Figure 4(c) indicates a two-roll symmetric pattern. The isotherms show that the fluid rises in the middle and descends along the sides. Figure 4(d), a perpendicular section, shows that the isotherms are stratified except at the ends, which is due to three-dimensional end effects.

Using the field variables at $Ra = 4 \times 10^4$ as the initial conditions, the Rayleigh number is increased in steps of 10^4, keeping all the other parameters fixed. The calculations indicate that the flow becomes unsteady at a Rayleigh number of 5×10^4. To investigate the dynamical nature of the flow field, the local

Table 1. Critical Rayleigh numbers as a function of aspect ratios as listed in [11]. The critical Rayleigh number for the present study was 2420 for aspect ratios of 2.4 and 1.2

A_x	A_z 1.00	2.00
2.00	2789	2276
2.50	2754	2222

variables were analyzed as a function of time in greater detail. Accordingly, the time series of the u-velocity at the nondimensional coordinate (1.753, 0.738, 0.918) was looked into. The spectral amplitudes of the time series of 8192 points and a nondimensional time step of 5×10^{-5} for a Rayleigh number of 6×10^4 are shown in Fig. 5(a). The time series for the same is shown in Fig. 5(c). Unless otherwise stated, the same local variables are used throughout this study.

The spectral amplitudes that are calculated using the standard Cooley–Tukey FFT algorithm indicate that the flow is periodic with a fundamental frequency of 44 nondimensional units, which corresponds to a frequency of 0.05 Hz in the experiments. The exact frequency was not reported in the experiments. However, all frequencies reported by Gollub and Benson [4] were of the same order of magnitude in the other similar cases. For example, for aspect ratios of 3.5 and 2.1 and $Ra = 3.6 \times 10^4$, the fundamental frequency was 0.067 Hz [4]. As seen in Fig. 5(a), there are higher harmonics to the fundamental frequency as well.

At a Rayleigh number between 7×10^4 and 8×10^4, the system undergoes a bifurcation to quasi-periodic flow. As seen in Fig. 5(b), the spectral amplitudes indicate that the new low frequency is added to the system at a Rayleigh number of 8×10^4. The additional low frequency was 0.003 Hz and is an order of magnitude lower than the other independent frequency. Figure 5(b) shows some closely spaced peaks that are the linear combinations and higher harmonics of the two fundamental frequencies. The time series for the quasi-periodic case shown in Fig. 5(d) shows the slow modulation of the amplitudes that typically occur if the two independent frequencies differ greatly in magnitude.

The quasi-periodic nature of the flow is more obvious when one examines the phase trajectories as shown in Fig. 6(a) for the same Rayleigh number. The two variables are the u-velocity at (1.753, 0.738, 0.918)

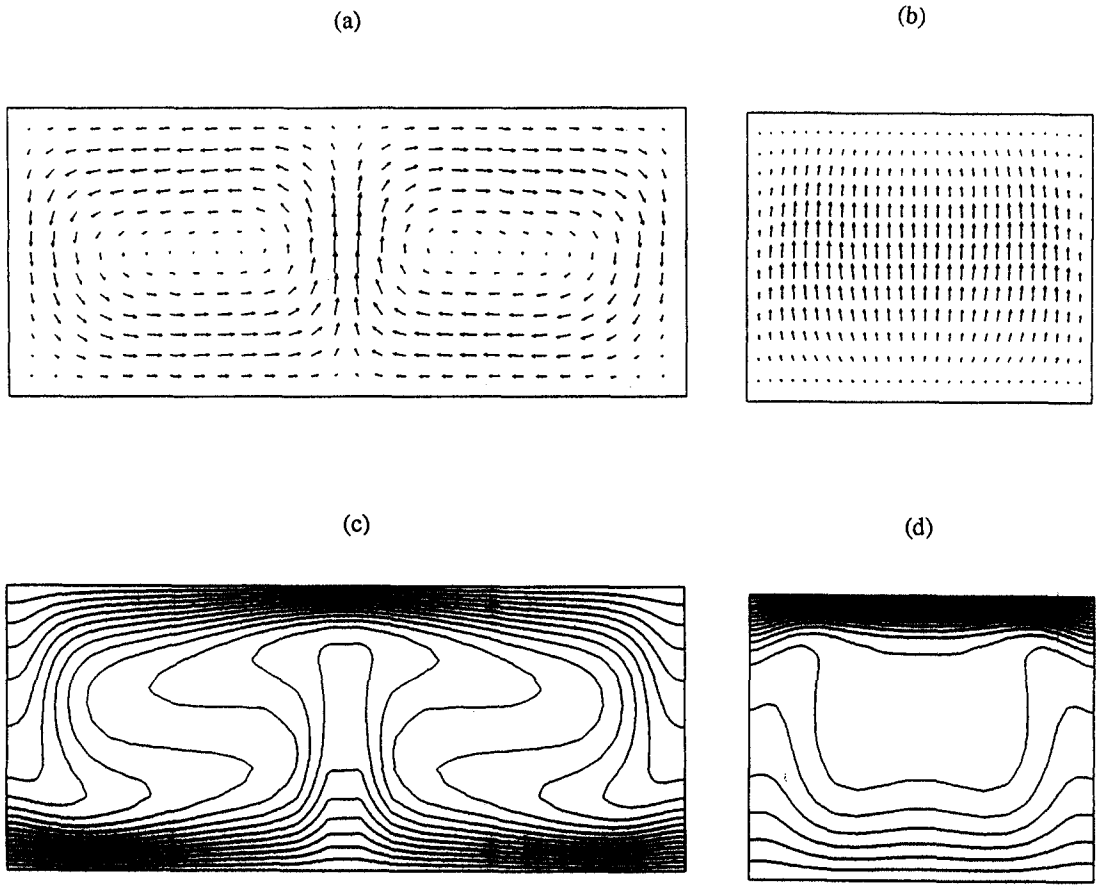

Fig. 4. Velocity vectors in (a) x–y plane for the section $z = 0.7$, (b) z–y plane for the section $x = 1.0$. Isotherms for sections (c) $z = 0.7$ and (d) $x = 1.0$. All velocities and isotherms are for $Ra = 4.0 \times 10^4$.

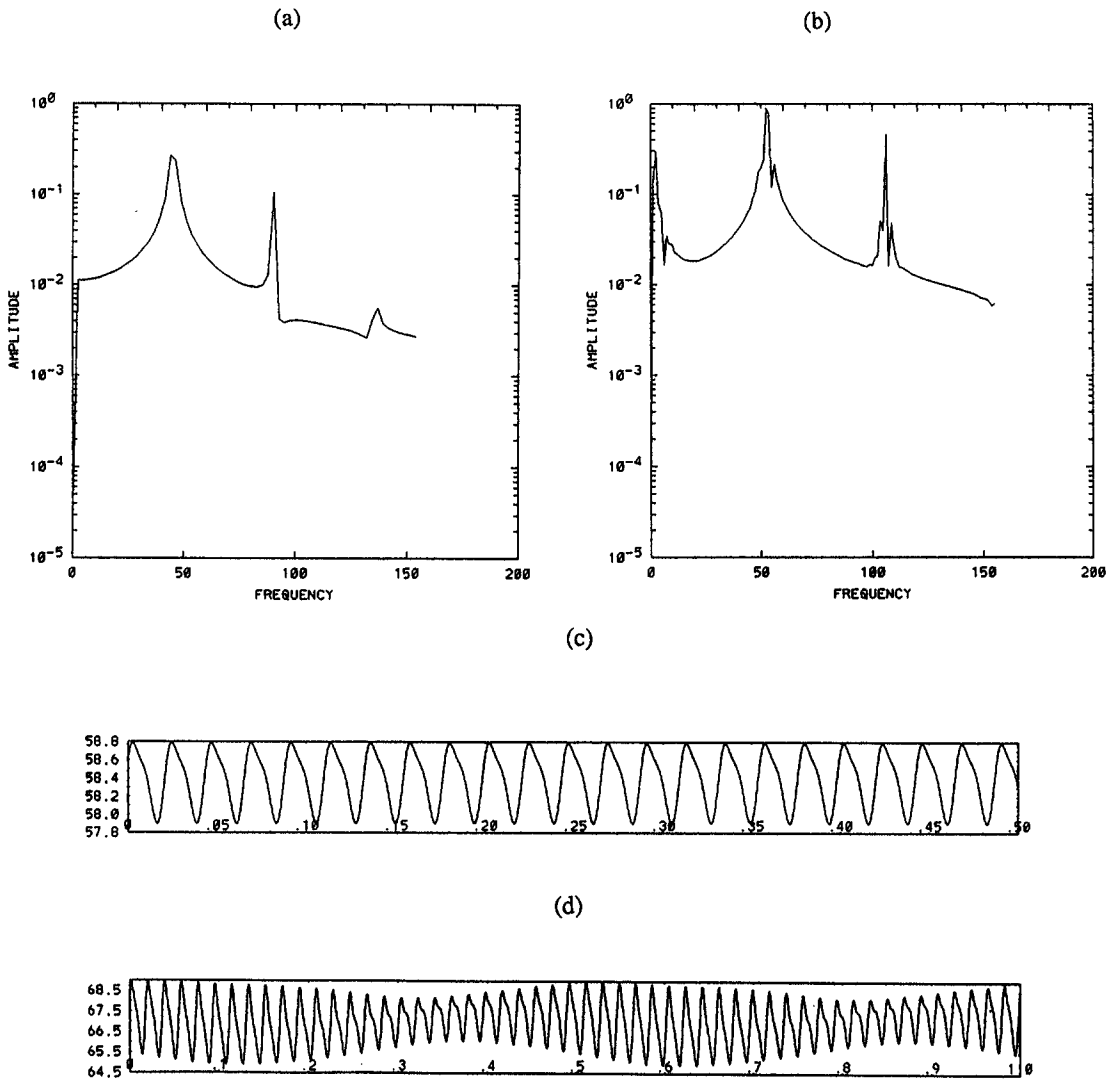

Fig. 5. u-Velocity oscillation amplitudes as a function of the frequency: (a) $Ra = 6.0 \times 10^4$; and (b) $Ra = 8.0 \times 10^4$. u-Velocity as a function of time (c) $Ra = 6.0 \times 10^4$; and (d) $Ra = 8.0 \times 10^4$. The u-velocity is for the co-ordinate (1.753, 0.738, 0.918).

and the v-velocity at (1.799, 0.716, 0.918). In geometrical terms, the trajectories appear to be embedded in a two-dimensional projection of a torus. This is expected when the dynamical behavior is quasi-periodic. In contrast, the phase trajectory for $Ra = 6 \times 10^4$, described earlier and for the same set of variables, is a simple closed curve for a system with one frequency [Fig. 6(b)].

We now look at the structure of the periodic and quasi-periodic flow in greater detail.

SPATIAL DISTRIBUTION OF SPECTRAL AMPLITUDES

The bifurcation sequences described thus far are identical to those reported in the experiments [4]. The critical Rayleigh numbers of the first two bifurcations are unfortunately not listed experimentally and cannot be compared. We do observe that the critical Rayleigh number of the first Hopf bifurcation is higher than the case with a smaller Prandtl number given in Mukutmoni and Yang [2]. This can be anticipated on physical grounds. A higher Prandtl number implies higher viscosity that would tend to damp out unsteadiness and correspondingly lead to higher critical Rayleigh numbers for the incipience of oscillatory convection.

It is therefore highly probable that the simulations thus far represent a real physically occurring phenomena. We are then justified in looking at the physics of the unsteady flow in greater detail. One very compact way of looking at this would be to study the spatial distribution of the spectral amplitudes for the different frequencies in the entire enclosure. It must be noted that, for small boxes, the dynamical behavior is simpler. More specifically, all variables at all points in

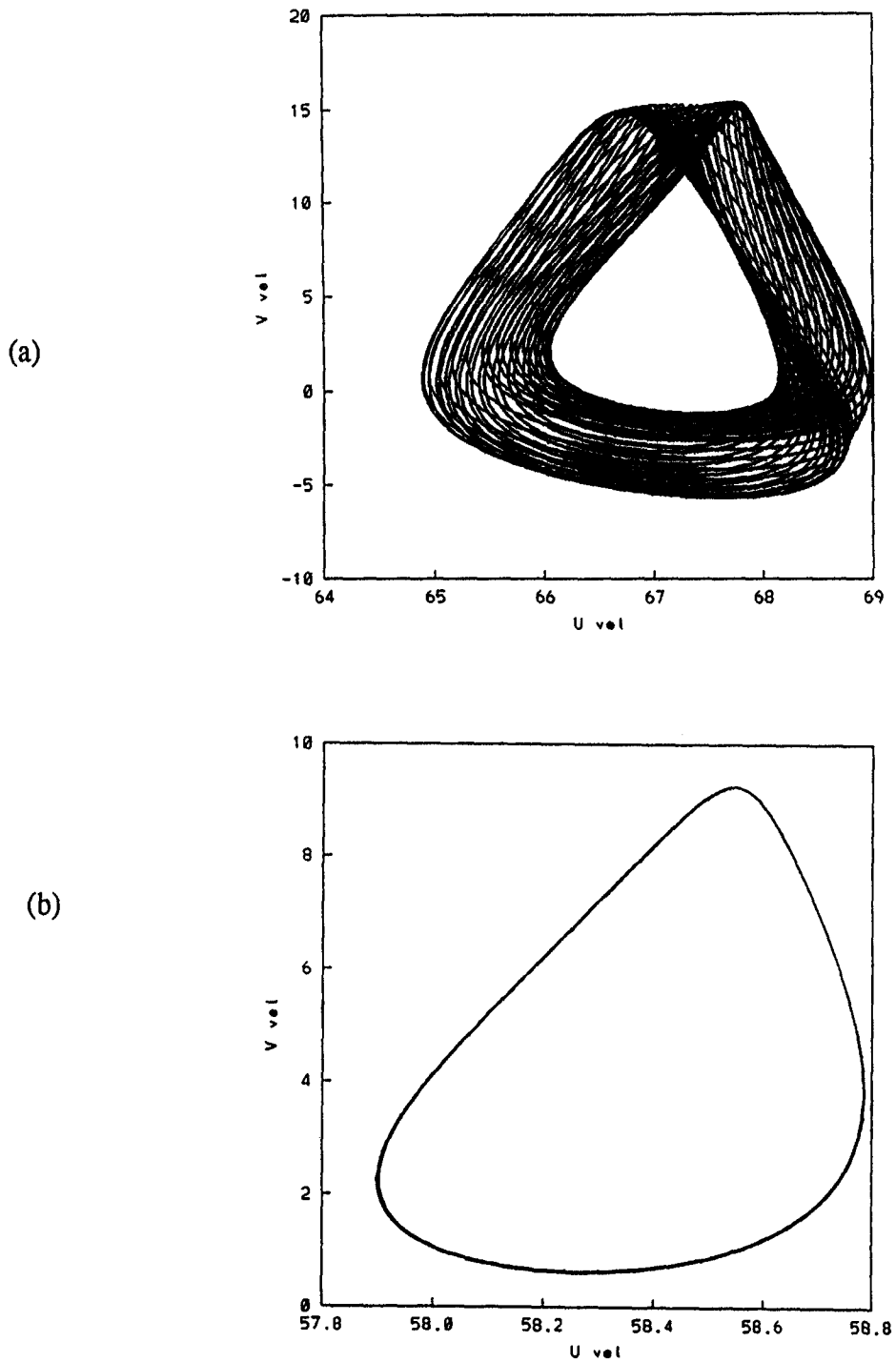

Fig. 6. The phase trajectory between the u and v velocities: (a) $Ra = 8.0 \times 10^4$; and (b) $\mathrm{Ra} = 6.0 \times 10^4$. The u-velocity is located at (1.753, 0.738, 0.918). The v-velocity is located at (1.799, 0.716, 0.918).

the box oscillate with the same frequency and share the same dynamical behavior. The field variables that represent the dynamical behavior of the nonlinear system can thus be selected arbitrarily. All spectral amplitude distributions in this study are for temperature oscillations.

Figure 7(a) shows the iso-surface of the spectral amplitudes for the fundamental frequency (44 non-dimensional units) of the temperature for a Rayleigh number of 6×10^4. The iso-surface [Fig. 7(a)] shows the physical domain where the spectral amplitudes and hence the oscillations are the strongest. Figure 7(b) shows a horizontal cross-section through the iso-surface. We find that the oscillation contours have

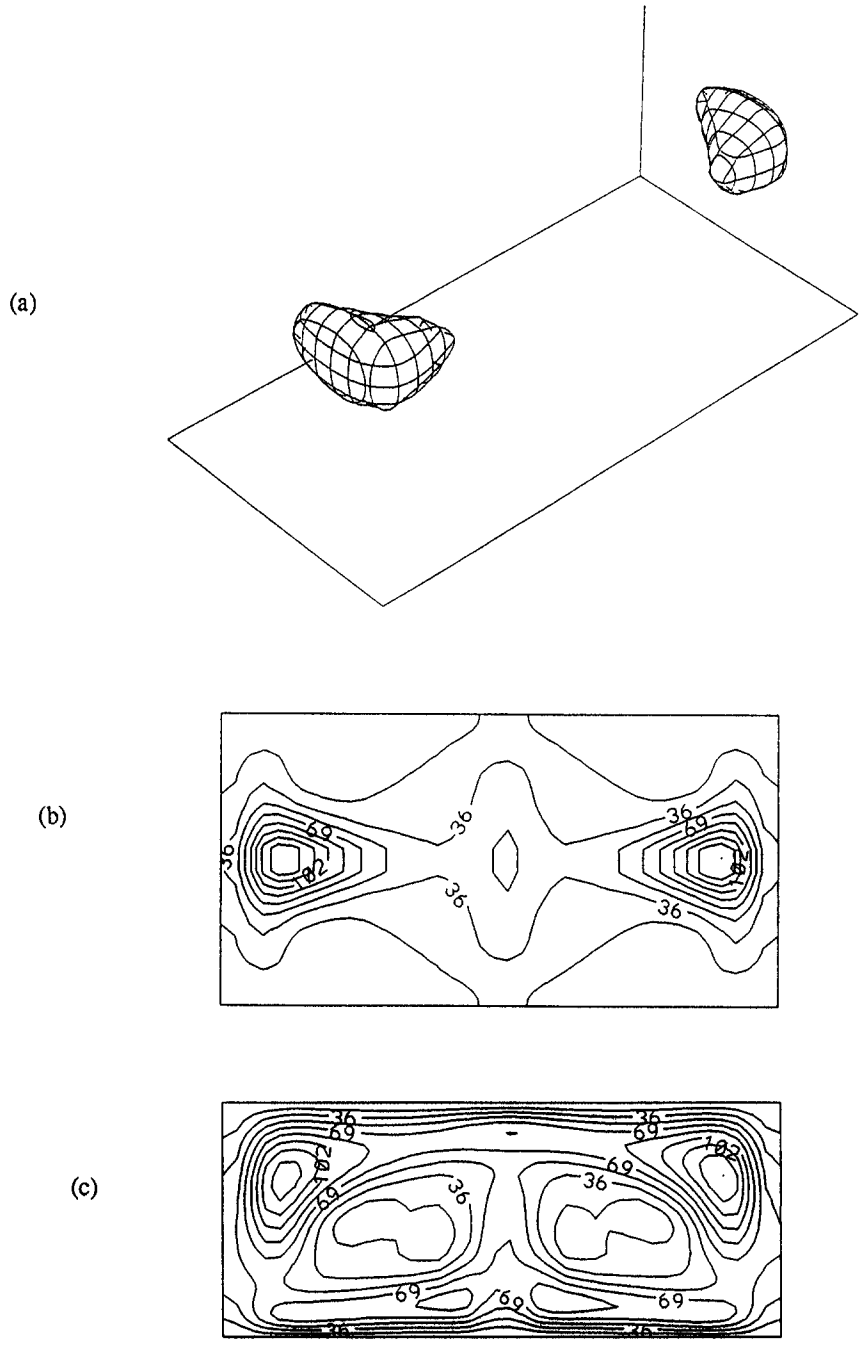

Fig. 7. Spectral amplitudes of temperature oscillations for nondimensional frequency of 44, $Ra = 6.0 \times 10^4$: (a) iso-surface plot for 0.8 times the maximum amplitude; (b) in the x–z plane at the section $y = 0.75$; and (c) in the x–y plane at the section $z = 0.61$.

a four-fold symmetry in the horizontal plane. The maximum amplitudes are located near the walls [Fig. 7(b)]. A vertical cross section through the iso-surface [Fig. 7(c)] reveals that the maximum amplitudes are at the top corners. It is obvious that the oscillations do not have a standing wave pattern along roll axes, which was found to be the case for lower Prandtl number fluids and larger geometrical aspect ratios [1, 2]. Rather, it consists of oscillations emanating from a source located in the upper corners of the horizontal mid-section perpendicular to the roll axis.

One can thus speculate that the fundamental oscillation for a small box is due to a "hydraulic jump" mechanism that has been proposed for side-heated cavities [12, 13]. In such a mechanism, the source of the oscillation was found to be near the corners as the flow moves along the isothermal vertical walls and abruptly hits the horizontal walls as it turns the corner.

The mechanism appears to be markedly different from the oscillatory instability proposed by Busse [14] and co-workers, for infinite RB convection. In such a case, time-dependence manifests itself as traveling waves propagating along the axes of the rolls.

The structure of the amplitudes of the higher harmonic was found to be almost the same and is therefore not shown. When the flow becomes quasi-periodic, we have two independent frequencies. The oscillation contours of the higher frequency (44 units) are virtually unchanged from the previous fundamental. The lower frequency (three units) was found to have a dramatically different structure. The iso-surface shown in Fig. 8(a) represents the volume in the box with the largest amplitudes of the second fundamental frequency. Unlike the larger frequency, the maximum oscillations are confined to the centerline that separates the two rolls and not near the corners.

Vertical cross-sections through the iso-surface [Fig. 8(b and c)] show that the maximum amplitude is restricted to a slab-like volume that divides the two rolls along its entire length. However, within this volume, the maximum amplitudes occur in a region just above the lower wall [Fig. 8(c)]. The four-fold symmetry of the oscillation amplitudes that was found in the other frequency is found in this case as well.

The lower frequency appears to be associated with slow and periodic increase and decrease of the dimensions of the two cells. The mechanism of the low frequency is the same as what was reported in Mukutmoni and Yang [3]. It is conceivable that, if the size of the cells were forced to remain unchanged using symmetry conditions on a quarter of the computational domain, the low frequency would be eliminated just as in the other study [3]. However, that was not attempted, since it would be a digression from the critical issues addressed in this paper.

REVERSION TO STEADY STATE

When the Rayleigh number is increased further, the flow field changes from quasi-periodic to steady state between the Rayleigh numbers of 1×10^5 and 1.1×10^5. The critical Rayleigh number reported in Gollub and Benson [4] for this transition is very close to the estimated critical Rayleigh numbers of the computations (Table 2). The transition to steady state, reported experimentally and reproduced numerically, is highly counter-intuitive. The general expectation is that the flow and temperature field would become more complex in the spatial and temporal sense as the Rayleigh number is increased. However, numerical and experimental evidence, in this case, seems to suggest the existence of at least one example that defies this trend.

Figure 9(a and b) shows the velocity field in two perpendicular vertical sections. Figure 9(a) represents the section in the x–y plane. A two-roll structure is observed that appears not to be very different from the two-roll structure seen before the bifurcation. However, the z–y section [Fig. 9(b)] reveals dramatic changes in the velocity field compared to the subcritical [Fig. 4(a and b)]. We observe a recirculating patch in the top-left region. The flow can be approximately described as having two unequal and non-symmetric rolls in the z–y plane. The mean flow has thus changed in subtle but significant ways. The flow as a result is more three-dimensional and there is periodicity in the z-direction as well.

The isotherms at the same corresponding sections [Fig. 9(c and d)] confirm the same trends. The contours in the x–y plane are relatively unchanged with the exception of a thinner thermal boundary layer. However, the one in the z–y plane [Fig. 9(d)] is very different from the previous case [Fig. 4(d)]. The reversion to steady state is confirmed in the time series of the u-velocity where an asymptotic approach to a steady state is evident [Fig. 9(e)]. It is therefore quite obvious that the bifurcation to steady state *also* resulted in a change in the spatial structure to a more complex three-dimensional form. Thus, the apparently paradoxical experimental and numerical results can now be reconciled within the existing framework.

Essentially, the reduction in its temporal complexity (quasi-periodic → steady state) is accompanied by an increase in its spatial complexities as a result of secondary flows due to bifurcation. It can then be argued that the overall complexity increases after the bifurcation, so there is no paradox or anomaly. Another way of looking at the phenomena would be to state that the secondary flow, as a result of the bifurcation, stabilized the unsteady convection of the subcritical. A real paradox would have arisen if it was found that the transition did not change the mean flow pattern and yet reverted to steady state, in which case our understanding of the transition phenomena would require revision. Fortunately, the transition observed is merely unusual or atypical and certainly does not require a re-evaluation of the scientific paradigm associated with the dynamical behavior of nonlinear systems.

FURTHER BIFURCATION TO OSCILLATORY FLOW

When the Rayleigh number is increased further, the flow becomes oscillatory at a Rayleigh number between 1.2×10^5 and 1.3×10^5. The mean velocity field is shown in Fig. 10(a–c) at three perpendicular sections. It is seen from the vertical sections [Fig. 11(a and b)], that there are no qualitative changes in the flow field compared to the subcritical flow [Fig. 9(a and b)] although the magnitude of the velocities is higher for the supercritical case. The horizontal section [Fig. 10(c)] indicates that the flow has organized

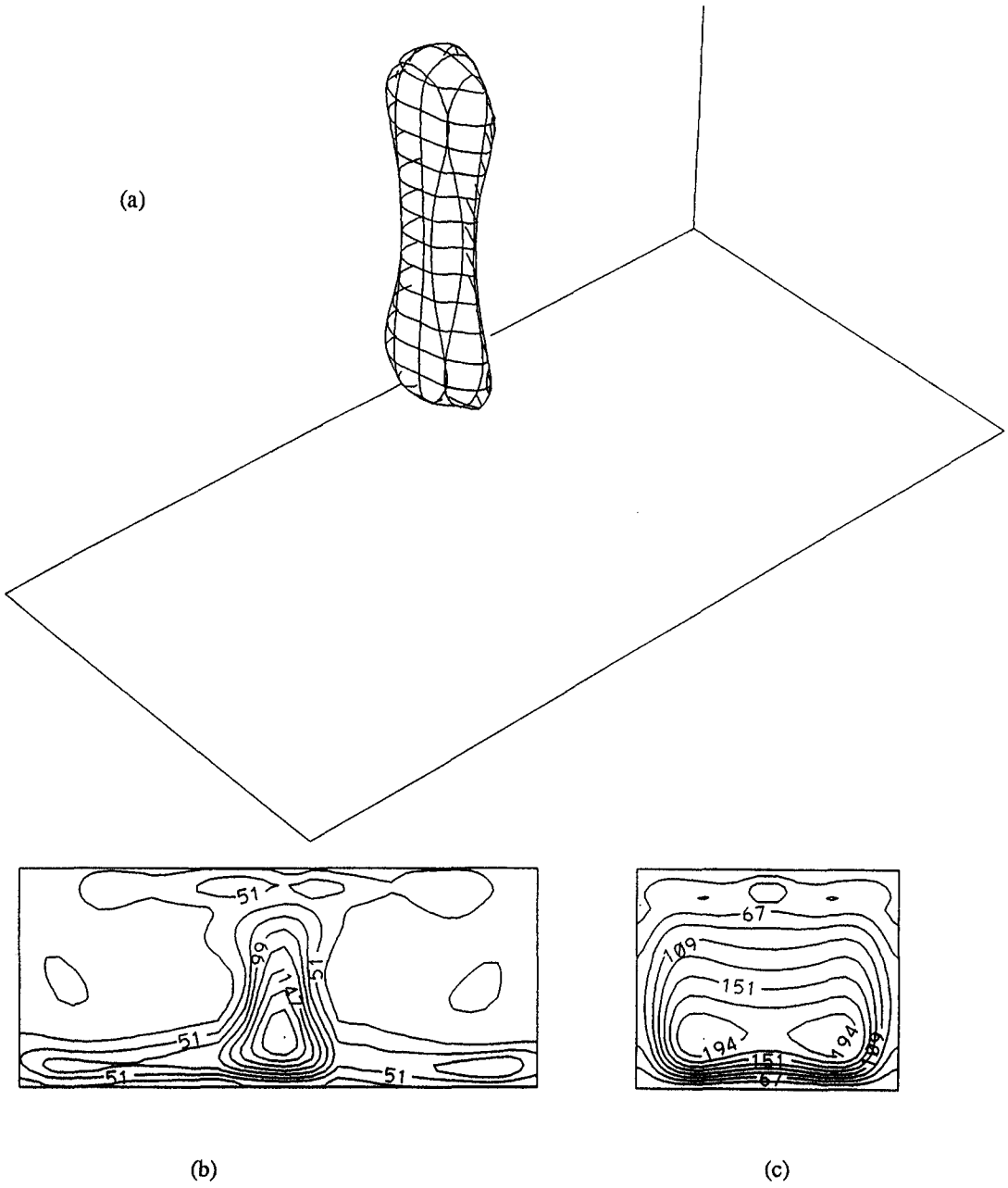

Fig. 8. Spectral amplitudes of temperature oscillations for nondimensional frequency of 3, $Ra = 8.0 \times 10^4$: (a) iso-surface plot for 0.8 times the maximum amplitude; (b) in the x–y plane at the section $y = 0.61$; and (c) in the z–y plane at the section $x = 1.2$.

Table 2. Comparison between experimentally observed sequence [4] and present study for $Pr = 5.0$, $A_x = 2.42$, $A_z = 1.23$

Experimental transition	Numerical transition	Critical Ra (experimental)	Critical Ra (numerical)
Steady state to periodic	Steady state to periodic	N/A	Between 5×10^4 and 6×10^4
Periodic to quasi-periodic	Periodic to quasi-periodic	N/A	Between 7×10^4 and 8×10^4
Quasi-periodic to steady state	Quasi-periodic to steady state	1.0×10^5	Between 1.0×10^5 and 1.1×10^5

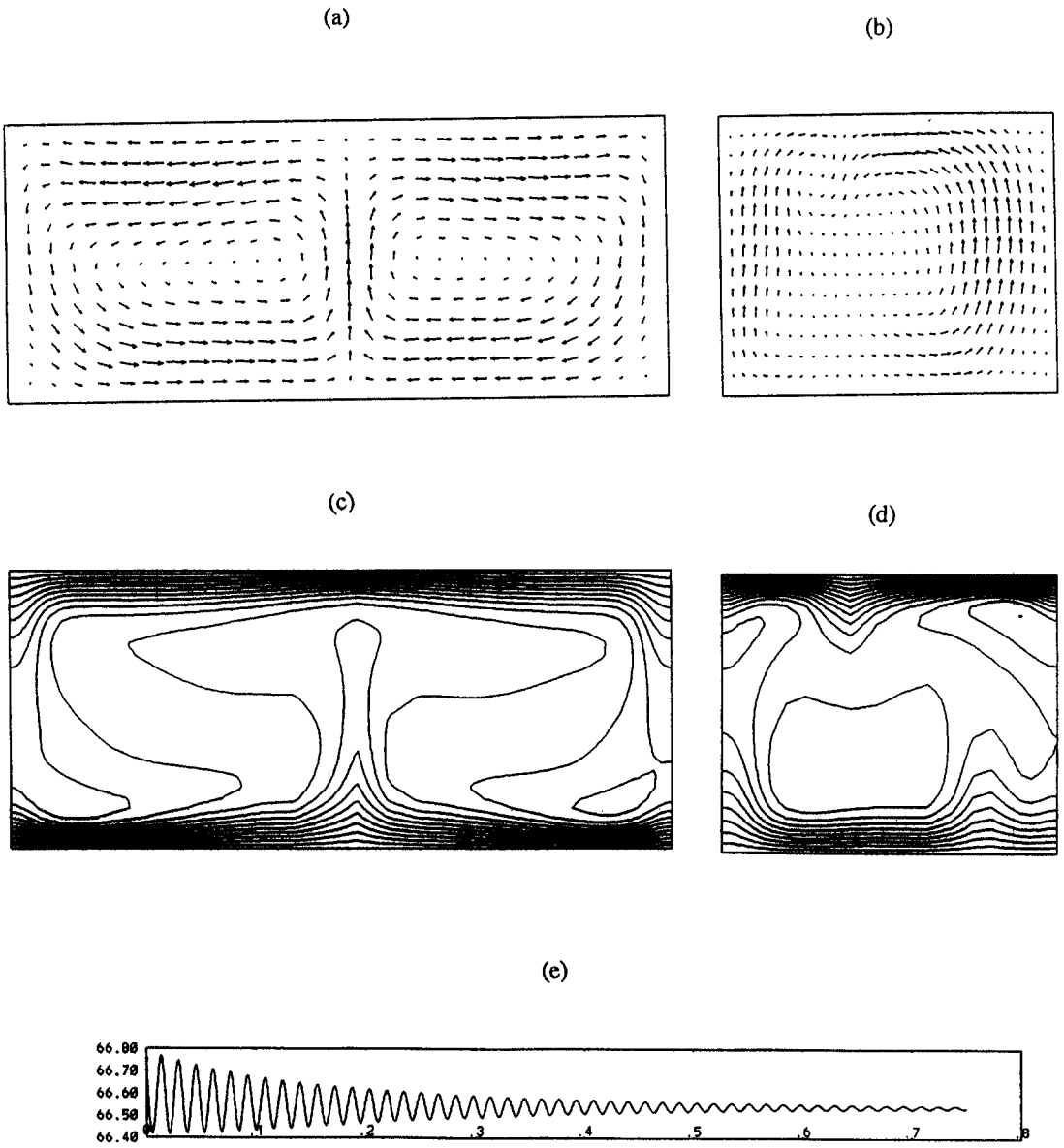

Fig. 9. Velocity vectors in (a) x–y plane for the section $z = 0.7$, (b) z–y plane for the section $x = 1.0$. Isotherms for sections (c) $z = 0.7$ and (d) $x = 1.0$. All velocities and isotherms are for $Ra = 1.1 \times 10^5$. (e) u-Velocity as a function time for $Ra = 1.1 \times 10^5$.

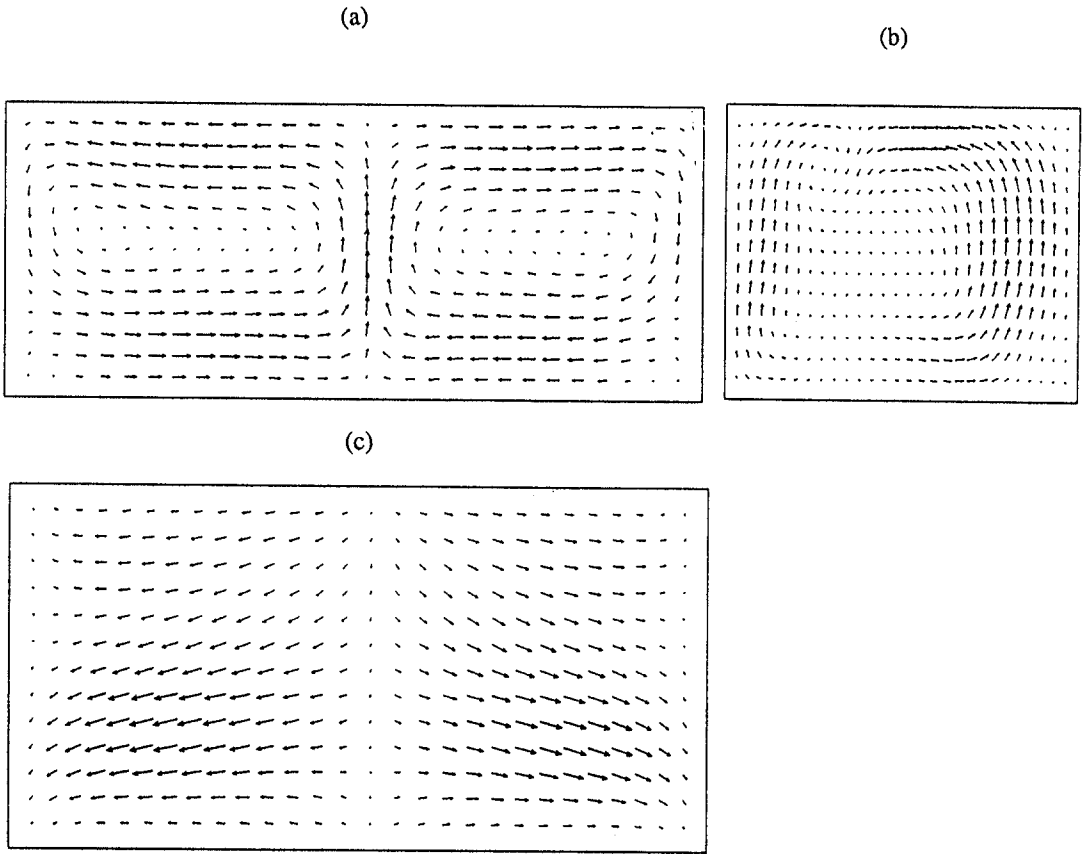

Fig. 10. Velocity vectors for the time-averaged velocity field for $Ra = 1.3 \times 10^5$: (a) x–y plane for the section $z = 0.7$; (b) z–y plane for the section $x = 1.0$; and (c) x–z plane for the section $y = 0.7$.

itself into four unequal sized rectangular cells in the planform.

A stationary oscillatory flow is seen for $Ra = 1.3 \times 10^5$, with the help of the velocity time series [Fig. 11(a)]. The spectral amplitudes indicate that a singly periodic state has been achieved and that the fundamental frequency has increased significantly to about 68 [Fig. 11(b)] compared to the lower Rayleigh number case. Previous experimental [4] and numerical [2] works indicated that the frequency increased slightly with an increase in Rayleigh number. However, such a sharp increase must be due to changes in the mean velocity and temperature field. A simple closed phase-trajectory confirms the single frequency dynamical behavior of the system [Fig. 11(c)].

Further computations at even higher Rayleigh numbers were not attempted in this study. According to the experiments [4], a spatial change in the mean flow field is documented. The dynamical behavior changes from quasi-periodicity to intermittency [4]. A study of the intermittency phenomena certainly demands our attention. However, an investigation at the higher Rayleigh number range would require a finer grid and will be the subject of a future study.

SUMMARY AND CONCLUSIONS

A numerical investigation was carried out for Rayleigh–Bénard convection in a rectangular box of aspect ratios 2.42 and 1.23 and a Prandtl number of 5.0, over a wide range of Rayleigh numbers. The simulations accurately modeled the experiments of Gollub and Benson [4]. The main goal of the simulations was to investigate the counter-intuitive transition from quasi-periodicity to steady state that was reported in the experiments and not adequately explained. The main conclusions in this study are the following:

(1) The numerical results were consistent with the limiting theoretical behavior near the critical Rayleigh number. In particular, the Nusselt number and the volume averaged kinetic energy depended linearly on ε. The critical Rayleigh number estimated by extrapolation agreed with the tabulated values available in the literature.

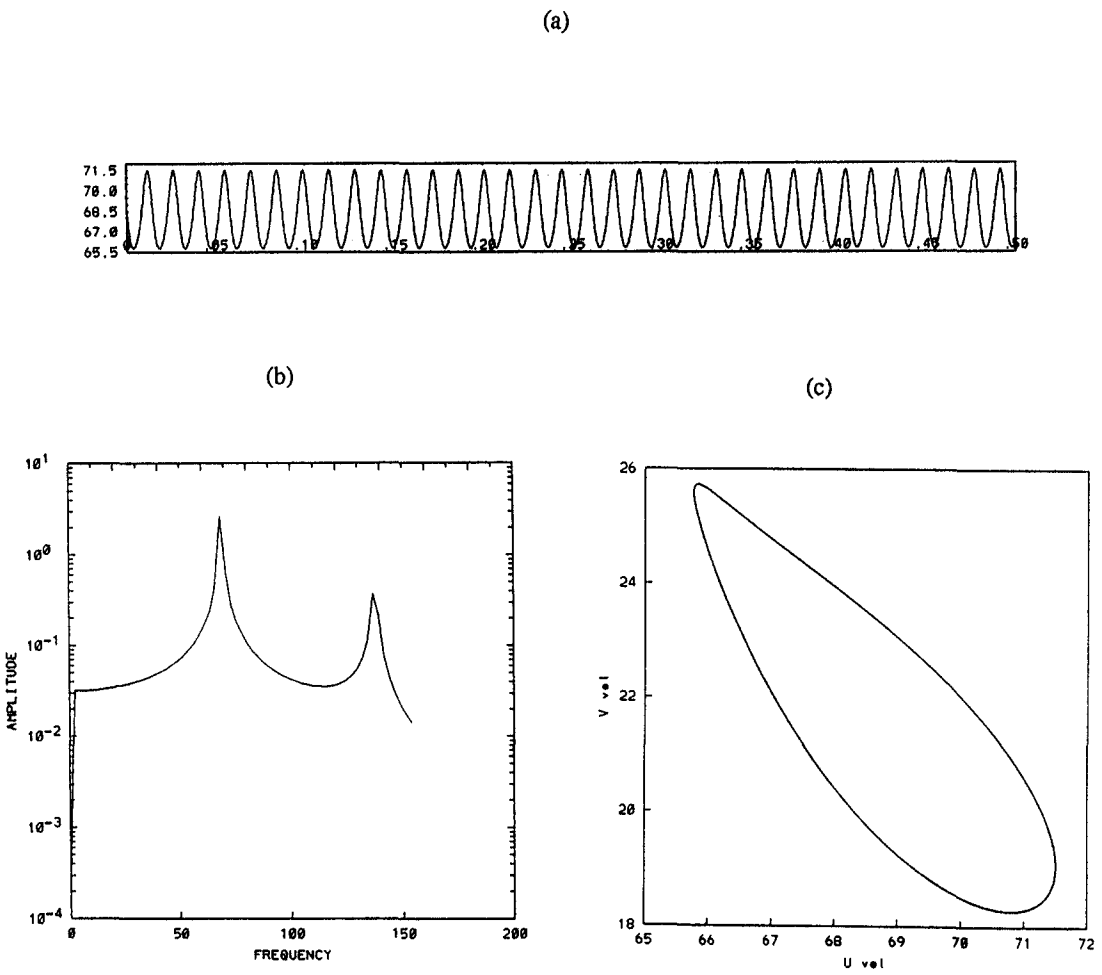

Fig. 11. (a) u-Velocity as a function of time; (b) u-velocity oscillation amplitudes as a function of frequency; and (c) u-velocity and v-velocity phase trajectory. All these are for $Ra = 1.3 \times 10^5$.

(2) The computations were able to reproduce the exact sequence of bifurcations reported in the experiments and also closely matched the critical Rayleigh numbers in cases where the information was available from experiments.

(3) The unsteady convection was analyzed in detail. The temperature oscillation amplitudes in the periodic regime showed a four-fold symmetry in the horizontal plane that was also observed in the time-averaged temperature and velocity fields. The maximum oscillation amplitudes were found to occur at the top corners along the vertical plane of symmetry perpendicular to the roll axes; which suggests a "hydraulic jump"-like mechanism.

(4) For the quasi-periodic regime, the added frequency was found to be an order of magnitude lower than the fundamental. The maximum oscillations occurred along the mid-plane that separates the rolls. This suggests that the low frequency component is responsible for the slow and pulsating increase and decreases of the cell dimensions.

(5) The bifurcation from quasi-periodic flow to steady state with an increase in the Rayleigh number was possible only because the spatial pattern of the flow field underwent changes as well. At a still higher Rayleigh number, the flow field changed from steady state to periodic and preserved the spatial structure in the time-averaged sense.

Acknowledgement—Computations were carried out in an Alpha workstation provided for by the Visualization Lab of the Naval Postgraduate School, Monterey, California.

REFERENCES

1. D. Mukutmoni and K. T. Yang, Wave number selection for Rayleigh–Bénard convection in a small aspect ratio box, *Int. J. Heat Mass Transfer* **35**, 2145–2159 (1992).
2. D. Mukutmoni and K. T. Yang, Rayleigh–Bénard convection in a small aspect ratio enclosure: part I—bifurcation to oscillatory convection, *J. Heat Transfer* **115**, 360–366 (1993).
3. D. Mukutmoni and K. T. Yang, Rayleigh–Bénard convection in a small aspect ratio enclosure: part II—bifurcation to chaos, *J. Heat Transfer* **115**, 367–376 (1993).

4. J. P. Gollub and S. V. Benson, Many routes to turbulent convection, *J. Fluid Mech.* **100,** 449–470 (1980).
5. P. Kolodner, R. W. Walden, A. Passner and C. M. Surko, Rayleigh–Bénard convection in an intermediate-aspect-ratio rectangular container, *J. Fluid Mech.* **163,** 195–226 (1986).
6. K. R. Kirchartz and H. Oertel Jr, Three-dimensional thermal cellular convection in rectangular boxes, *J. Fluid Mech.* **192,** 249–286 (1988).
7. K. T. Yang, Transitions and bifurcations in laminar buoyant flows in confined enclosures, *J. Heat Transfer* **110,** 1191–1204 (1988).
8. F. P. Incropera and D. P. DeWitt, *Introduction to Heat Transfer*. Wiley, New York (1985).
9. K. G. T. Hollands and G. D. Raithby, *Handbook of Heat Transfer Fundamentals* (Edited by W. M. Rohsenow, J. P. Hartnett and Z. N. Ganic). McGraw-Hill, New York (1985).
10. S. Chandrasekhar, *Hydrodynamic and Hydromagnetic Stability*. Oxford University Press, Oxford (1961).
11. R. P. Behringer, Rayleigh–Bénard convection and turbulence in liquid helium, *Rev. Mod. Phys.* **57,** 657–687 (1985).
12. S. Paolucci and D. R. Chenoweth, Transition to chaos in a differentially heated vertical cavity, *J. Fluid Mech.* **201,** 379–410 (1989).
13. G. N. Ivey, Experiments on transient natural convection in a cavity, *J. Fluid Mech.* **144,** 389–401 (1984).
14. F. H. Busse, Non-linear properties of thermal convection, *Reps Prog. Phys.* **41,** 1929–1976 (1978).